AIAA JOURNAL
Vol. 46, No. 8, August 2008

Mach 3 Shock Wave Unsteadiness Alleviation Using a Negative Corona Discharge

P.-Q. Elias* and B. Chanetz†
ONERA, 92190 Meudon, France
S. Larigaldie‡ and D. Packan§
ONERA, 91761 Palaiseau, France
and
C. O. Laux¶
Ecole Centrale Paris, 92290 Chatenay–Malabry, France

DOI: 10.2514/1.34674

Experiments to stabilize an unsteady Mach 3 shock wave on a truncated body fitted with a central spike have been conducted in the ONERA R1Ch blowdown wind tunnel. Stabilization was achieved by means of a negative corona discharge created at the tip of the spike. Several runs have been performed, with a freestream unit Reynolds number varying in the range of [0.910^7–3.510^7 m^{-1}]. Onboard discharges can be generated using an ac or dc potential between the tip of the spike and the truncated face, similar to the setup of Kuo (Kuo, S., Kalkhoran, I., Bivolaru, D., and Orlick, L., "Observation of Shock Wave Elimination by a Plasma in a Mach = 2.5 Flow," *Physics of Plasmas*, Vol. 7, No. 5, 2000, pp. 1345–1348.). Without discharge, for a certain spike length we observe that, depending on the Reynolds number or the surface state of the spike, the shock front is unsteady or not. In the case of a naturally unsteady shock front, we observe a complete stabilization of the shock when a negative discharge is generated at the spike tip. With positive discharges, the effect is weaker. Both discharges are pulsed, and their input power is less than 1 W. Discharge imaging and current measurements indicate that the negative discharge is a Trichel-pulsed corona discharge, whereas the positive discharge is a streamer discharge. An order-of-magnitude analysis and infrared imaging indicate that continuous volume and surface heating are negligible. To explain the stabilization mechanism, we argue that the pulsed discharge acts as an acoustic source tripping the boundary layer, thus leading to a bypass transition to turbulence.

Nomenclature

C_D = mean drag coefficient, 1
c_p = air specific heat, $J \cdot K^{-1} \cdot kg^{-1}$
D = front section diameter, m
$D1$ = main section diameter, m
f = pulsation frequency, Hz
I_D = discharge current, A
k = groove depth, m
L_S = spike length, m
M_e = external Mach number, 1
M_0 = freestream Mach number, 1
n_L = Loschmidt number, m^{-3}
n_0 = freestream density number, m^{-3}
P_{in} = discharge input power, W
Re_u = unit Reynolds number, m^{-1}
r = image correlation coefficient, 1
S = reference area, m^2
St = Strouhal number, 1
T_0 = freestream temperature, K
U_b = breakdown voltage, V
U_D = discharge voltage, V
u_0 = freestream flow velocity, $m \cdot s^{-1}$
ΔT = freestream temperature increase, K
δ_1 = boundary-layer displacement thickness, m
μ_0 = freestream viscosity, $kg \cdot m^{-1} \cdot s^{-1}$
ρ_0 = freestream volumetric mass, $kg \cdot m^{-3}$
σ = image correlation coefficient standard deviation, 1

Received 19 September 2007; revision received 4 March 2008; accepted for publication 4 March 2008.

*Research Scientist; paul-quentin.elias@onera.fr.
†Deputy Director, Département d'Aérodynamique Fondamentale et Expérimentale.
‡Senior Scientist, Département Mesures Physiques.
§Research Scientist, Département Mesures Physiques.
¶Professor, Laboratoire EM2C CNRS-UPR 288. Associate Fellow AIAA.

I. Introduction

SEVERAL key issues, such as sonic boom or high fuel consumption levels, still hinder the development of economically and environmentally viable supersonic airliners. The optimization and refinement of existing technologies is the primary path to overcome these issues. The assessment and development of new technological concepts is also another path that could provide stepwise performance increases. Among these new concepts, the use of nonequilibrium gas discharges in supersonic airflows has received considerable attention for the past decade. Russian studies released in the mid-1990s suggested that these discharges, also termed cold plasmas, could significantly alter supersonic airflows [1] and thus lead to better aerodynamic performances.

These so-called plasma effects, in particular their thermal or nonthermal nature, have been the object of numerous experimental investigations.

The review paper by Bletzinger et al. [2] suggests that the observed plasma effects are mainly of a thermal nature. A considerable amount of work has been devoted to the generation of plasma in supersonic wind tunnels using outboard or onboard generation devices. For example, in their studies of nonequilibrium discharges in front of a wedge and a cone, Palm et al. [3] demonstrated that the plasma has a very weak thermal effect on the conical shock wave, consistent with the low electrical input power, and that the shock angle increase observed on a wedge is consistent with a plasma-induced boundary-layer heating. Shang [4] used a counterflowing plasma jet on a hemispherical model. Counterflow jets are known to reduce the drag. Shang observed an increased drag reduction when the counterflow

jet is ionized. However, numerical simulations of the flow show that the effect is similar to hot air injection. Bivolaru and Kuo [5,6] studied a conical plasma aerospike produced with high-power electrical discharges around a thin spike. When the discharge was turned on, they observed that the shock front turned from a blunt shock to a conical shock. In the meantime, they recorded a 2.5-fold increase in the gas temperature measured at the lower third of the conical body. Contrary to Bivolaru and Kuo's conclusion, we believe that the gas heating hypothesis is sufficient to explain their observations.

However, thermal effects alone do not seem to explain certain experimental observations. In particular, Kuo et al. [7] and Kuo and Bivolaru [8] observed noticeable shock dispersion when switching on a discharge on a truncated model fitted with a central spike. These effects were observed when the spike was negatively biased, with an average power input of about 100 W. According to the authors of [8], this power level is too low to explain the shock dispersion. This observation is very interesting because it suggests a nonthermal coupling between the plasma and the supersonic airflow. Moreover, the shock wave dispersion resulting from this coupling may produce a significant decrease in the wave drag. Consequently, using a model design similar to the one proposed by Kuo and Bivolaru, we have sought to obtain a coupling between the plasma and the flow and to investigate its properties. For this purpose, we have devised an experimental setup with time-resolved diagnostics. First, the flow without discharge has been characterized. Second, evidence of a plasma flow coupling has been sought by varying the flow and the plasma characteristics. Third, the coupling characteristics have been investigated using aerodynamics and plasma diagnostics.

In this paper, we report our investigations of the interaction between an unsteady flow and a corona discharge. The experimental details are given in Sec. II. The baseline flow studies are described in Sec. III. The plasmaflow interactions are presented in Sec. IV. A discussion is proposed in Sec. V.

II. Experimental Setup

The work presented in this paper was conducted with the ONERA R1Ch blowdown wind tunnel. This facility delivers a $M_0 = 3$ flow. The exit nozzle is 330 mm in diameter. A run lasts around 10 s, during which the stagnation pressure and temperature are continuously recorded. As a preliminary study, the spatial profiles of the Mach number and stagnation temperature at the location of the model were measured. The spatial variations of the Mach number and stagnation temperature were measured to be less than 1%. The freestream turbulence intensity of the wind tunnel is around 1%. The test model is a 60-deg truncated cone with a central spike. The model outer shell and the central spike are electrically insulated from each other and serve as electrodes, as shown in Fig. 1. The truncated face diameter is $D = 35$ mm and the body diameter is $D1 = 70$ mm. Spikes of various lengths can be attached to the model. In this paper, we report on the work conducted with a single spike of diameter $d = 7$ mm and length $L_S = 16.1$ mm, giving an aspect ratio of $L_S/D = 0.46$. Electrical power is provided by one of two power supplies. The first is an ac power supply similar to the one used by Kuo and Bivolaru [8]. It provides a 50-Hz ac output voltage, varying from 0 to 7 kV or from 0 to −7 kV depending on the diode polarity. Its principle is sketched in Fig. 1. The second one is a 0–12 kV/20 mA dc power supply. The output voltage is either negative or positive.

To investigate plasmaflow interactions, fast aerodynamic and electric measurements are employed. A high-speed camera records

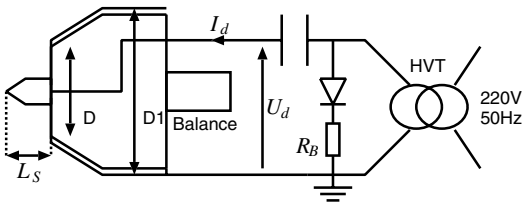

Fig. 1 Experimental setup.

the shock wave pattern through a standard schlieren system. The recordings are sampled at 12,500 frames per second and last for about 4 s. The exposure time is 4 μs. The camera has a built-in acquisition system that allows synchronous recording of the discharge voltage. For a given run, around 50,000 schlieren images are recorded. Theses images can be quantitatively compared by computing the image correlation coefficient, r. This coefficient is computed by selecting a reference image in the batch. The image is coded by a matrix, A_{ij}^{ref}. Then, for each image of the batch coded by the matrix A_{ij}^{k}, the correlation r with the reference image is given by

$$r(\text{ref};k) = \frac{\left(\sum_{i,j} a_{ij}^{\text{ref}} a_{ij}^{k}\right)^2}{\sum_{i,j}\left(a_{i,j}^{\text{ref}}\right)^2 \sum_{i,j}\left(a_{i,j}^{k}\right)^2} \tag{1}$$

where $a_{ij} = A_{ij} - m$, with m as the matrix mean value. The correlation coefficient is relative to a given reference image of the batch. Its time evolution gives information on the state of the flow. If r is roughly constant, it shows that all schlieren images are similar, meaning that the main features of the flow are stable. A particular case is when the coefficient r is roughly equal to 1. It means that all schlieren images are close to the reference image.

The drag on the model is measured with a six-component balance. The balance bandwidth is below 800 Hz. However, its signal is sampled at 20 kHz. A high-voltage probe and a Pearson coil measure the discharge voltage and current, respectively. Their outputs are sampled at 10 MHz on a four-channel LeCroy oscilloscope. Additional data on the discharge are obtained using optical diagnostics. Digital cameras provide time-integrated pictures of the discharge. An intensified charge-coupled device camera (ICCD) operating at four frames per second (fps) has also been used to observe the discharge with exposure times from 10 to 100 μs. A FLIR infrared (IR) camera operating at 25 fps has also been employed to measure the surface temperature of the model.

In this work, the main adjustable parameter is the freestream unit Reynolds number, $Re_u = \rho_0 u_0/\mu_0$. The maximum voltage of the circuit is fixed, as well as the wind-tunnel Mach number. First, we characterized the airflow properties as a function of the unit Reynolds number. Then, we studied plasmaflow interactions by switching on the plasma during a run. In this case, the airflow was monitored with the fast camera and the discharge with the electrical probes. The results are synchronized using the fast camera start signal triggering the LeCroy oscilloscope.

III. Baseline Flow Characterization

Without discharge, the steadiness of the flow depends on the reduced spike length, L_S/D. For $L_S/D \leq 0.40$, the model generates a steady bow shock [9]. For $0.40 \leq L_S/D \leq 0.80$, the flow is unsteady [10]. Mair [11] reported the observation of flow unsteadiness on spiked blunted bodies. A detailed numerical study of the flow unsteadiness was published by Feszty et al. [12]. Here, the reduced spike length is set to $L_S/D = 0.46$.

For $L_S/D = 0.46$, without discharge, periodic inflations and deflations of the shock front are observed, as shown in the successive schlieren images presented in Fig. 2 that cover a period of the unsteadiness. The fast schlieren recordings can be used to estimate the reduced pulsation frequency, $St = fL_S/u_0$. Assuming that five to six schlieren images are recorded during the pulsation period, the reduced frequency is $St = 5 \pm 1 \times 10^{-2}$.

A more quantitative determination of the reduced frequency is sought using statistical and spectral analyses of the balance signal recorded during a run. First, the mean drag coefficient C_D measured with the balance is $C_D = 0.854 \pm 0.005$ for unit Reynolds numbers between 1.1×10^7 and 2.1×10^7 m^{-1}. Second, to check that the pulsation frequency appears in the power spectral density (PSD) of the fluctuating part of the balance measurement, a 150-PSI-A Kulite pressure sensor (bandwidth 300 Hz–20 kHz) is mounted on the truncated front section, halfway between the spike base and the outer shell, for a run without plasma. In fact, to avoid uncontrolled arcing

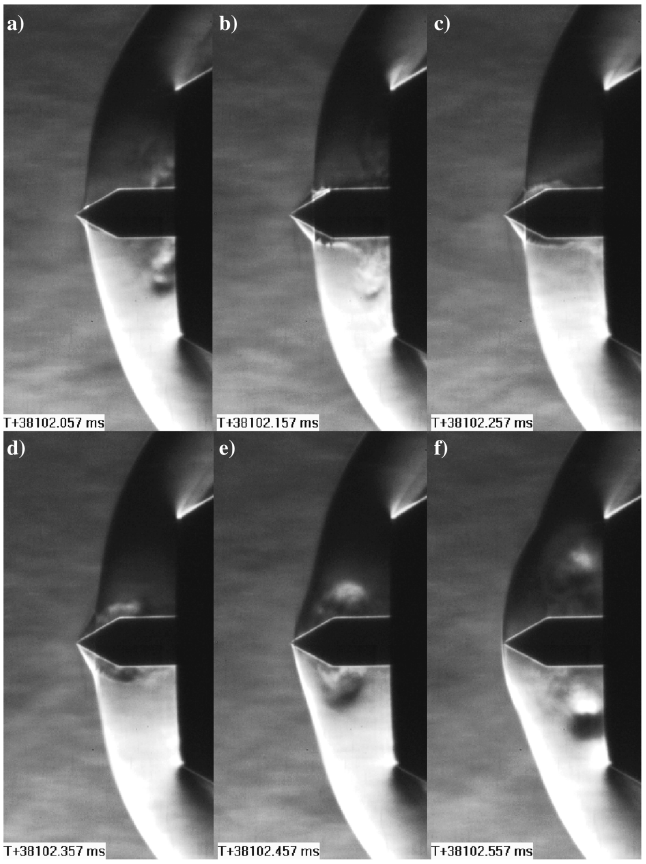

Fig. 2 Schlieren images, sampled every 100 μs (exposure time 5 μs, $Re_u = 1\text{–}1.5 \times 10^7$ m^{-1}, $n_0/n_L = 0.1\text{–}0.15$, $T_0 = 113$ K, no discharge).

between the sensor and the spike, we did not use the sensor with the high voltage turned on. Because the shock pulsation induces strong fluctuations on the front section pressure, a comparison of the pressure signal with the balance signal indicates whether the pulsation frequency appears in the balance signal spectra. In Fig. 3, the piezoelectric pressure sensor PSD and the balance signal PSD are compared. For $St \times 10^2 > 1$, the peaks of both PSDs are in good agreement, although their relative amplitudes are markedly different. In fact, the balance damps the high-frequency modes, because its transfer function is qualitatively equal to a second-order system with a 800-Hz cutoff frequency. For $St \times 10^2 < 1$, the balance displays

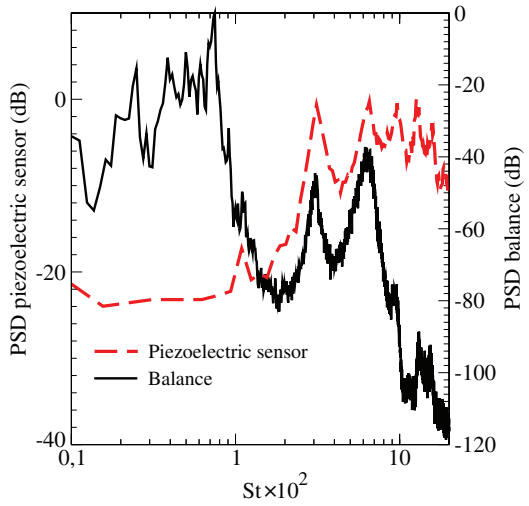

Fig. 3 Comparison of the balance and piezoelectric sensor PSDs, without discharge ($Re_u = 2.17 \times 10^{-7}$ m^{-1}, cutoff frequency $St_c \times 10^2 = 24$).

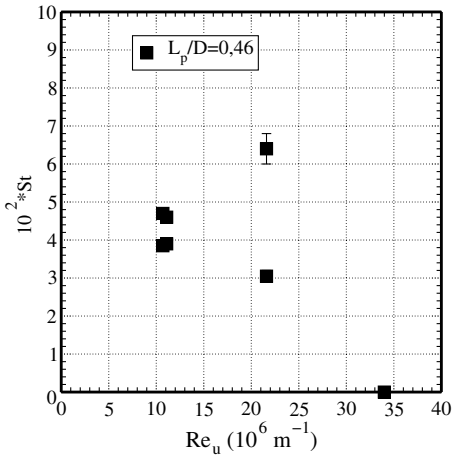

Fig. 4 Pulsation frequency ($L_S/D = 0.46$, no discharge).

several peaks that are not visible in the piezoelectric sensor. This is probably due to the lower bandwidth limit of the sensor and also to the mechanical response of the balance. The agreement observed between these two signals in the high-frequency region shows that the balance PSD peaks can be used to determine the pulsation frequency. Note that the multiple peaks observed at high frequencies in the pressure sensor PSD trace are harmonics of the main pulsation, because their frequencies are multiples of the first peak frequency, around $St \times 10^2 \simeq 3.1$. In Fig. 4, the reduced pulsation frequency peaks measured on the balance PSD are plotted vs the unit Reynolds number. For a given Reynolds number, two points are given corresponding to the first two peaks measured in the high-frequency region of the balance PSD. For $Re_u = 3.4 \times 10^7$ m^{-1}, no high-frequency peak is observed. In this case the fast schlieren images indicate that the shock front is completely stable (as shown in Fig. 7b). Thus, we set $St = 0$. Above a critical unit Reynolds number between $Re_u = 2.2 \times 10^7$ and 3.4×10^7 m^{-1}, the shock front is stable, whereas it is unsteady below.

This dependence on the unit Reynolds number suggests that turbulence effects may have a role in the stabilization of the shock pulsation. To investigate this point, the schlieren images are carefully examined. In Figs. 2c–2e, expanding contrasted zones are observed around the spike conical tip. This indicates that the density is different in these zones, likely the sign of a recirculating flow. In Fig. 2f, the contrasted zones are located symmetrically around the spike. This could indicate the presence of a toroidal vortex shed by the aforementioned recirculating bubble. The sheared flow in the recirculating bubble is very sensitive to external perturbations. In supersonic wind tunnels, the freestream perturbation level is quite high because of the noise radiated from the turbulent nozzle boundary layer [13]. Thus, transition to turbulence is likely to occur in this region.

Consequently, the onset of turbulence in the vicinity of the spike tip and its influence on the flow should be investigated. For this purpose, small surface defects have been machined on a spike of dimensions identical to those of the base spike, as shown in Fig. 5. The goal is to trigger the transition to turbulence at the very beginning of the spike boundary layer. The surface defects consist of evenly spaced grooves along the first 2 mm of the spike. The grooves' depth is around 100 μm. Van Driest and Blumer [14] give the groove depth k required to trigger the transition to turbulence:

$$\frac{k}{\delta_1} = 32,4\sqrt{1 + 0,2M_e^2}\left(Re_u^e \delta_1\right)^{-1/2}$$

Here, δ_1 is the displacement thickness and M_e the Mach number above the boundary layer. For unit Reynolds numbers between 6.4×10^6 and 3.3×10^7 m^{-1}, this gives a defect height between 10 and 50 μm. The actual height is around 100 μm because of the limitations of the machining process. Nevertheless it is high enough to ensure the transition to turbulence at the beginning of the spike.

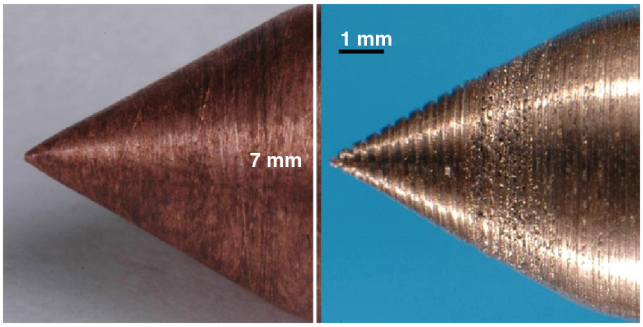

Fig. 5 Comparison between the smooth spike (left) and the rough spike (right).

Several runs were performed at different unit Reynolds numbers with the two spikes. The state of the flow is quantitatively described by computing the image correlation. For each run, the reference image is chosen to correspond to the innermost position of the shock, as shown in Figs. 2 and 3. In this case, the shock position is qualitatively similar to the stable case at a higher Reynolds number (see Fig. 7b, for example). For each run, the standard deviation, σ, of the correlation coefficient is computed to quantitatively measure the stability of the schlieren images of the flow. In two cases, the pressure sensor standard deviation is also computed. Results are given in Fig. 6. For $Re_u \simeq 10^7$ m^{-1} and $Re_u = 1.4 \times 10^7$ m^{-1}, the shock front around the model with the smooth spike is unsteady, whereas

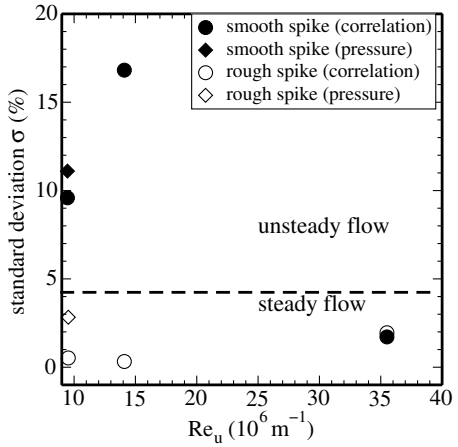

Fig. 6 Image correlation (circles) and pressure (diamonds) standard deviation for the smooth and rough spikes vs the unit Reynolds number.

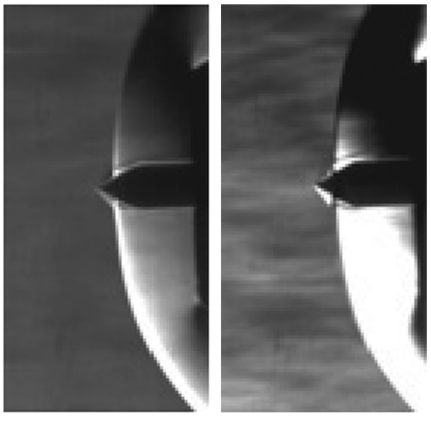

a) **b)**

Fig. 7 Schlieren images of the flow for $L_s/D = 0.46$ without discharge: a) rough spike ($Re_u = 9.53 \times 10^6$ m^{-1}, exposure 19 μs), and b) smooth spike ($Re_u = 3.4 \times 10^7$ m^{-1}, exposure 19 μs).

the shock front around the model with the rough spike is stable. A schlieren image of the flow with the rough spike for $Re_u \simeq 10^7$ m^{-1} is given in Fig. 7a. It is very close to the case with the smooth spike for $Re_u \simeq 3.4 \times 10^7$ m^{-1}, as shown in Fig. 7b. Thus, the unsteadiness of the shock is linked to the state of the boundary layer on the conical tip of the spike. The onset of turbulence in the boundary layer stabilizes the shock pulsation. The turbulence onset occurs if the unit Reynolds number is high enough or if small surface defects trip the boundary layer. As a first step toward understanding this, we underline that the separated region created at the spike tip should be strongly influenced by the state of the boundary layer at the detachment point. For example, a turbulent boundary layer can sustain stronger adverse pressure gradients than a laminar boundary layer [15]; turbulent recirculating bubbles are shorter than laminar ones. Thus, the global stabilization of the shock pulsation may have its source in the stabilization of the recirculating zone created by a shock-boundary-layer interaction on the spike conical tip.

This study of the flow without discharge is the first step toward understanding a possible plasmaflow interaction, because it clarifies the unsteadiness mechanism.

IV. Flow-Discharge Interaction

In a second step, discharges are generated in a reference flowfield with a $L_S/D = 0,46$ smooth spike. The flow unit Reynolds number ranges from 9.5×10^6 to 1.5×10^7. In this range, the flow is always unsteady, as shown in Fig. 6. The freestream temperature is $T_0 = 120 \pm 4$ K. The ac circuit is switched on during the run, and the flowfield is monitored with the fast camera. Both polarities have been tested. In both cases, when the voltage magnitude, U_D, exceeds the breakdown voltage, U_b, we observe a discharge located in the vicinity of the spike tip, upstream of the main bow shock. In the negative discharge, the emission pattern is located in the immediate vicinity of the spike tip, whereas in the positive case it is more diffuse and covers a wider volume. The electrical characteristics of both discharges show repetitive current pulses when the discharges are on. In Fig. 8, typical current pulses recorded in both polarities are displayed. Pulse amplitudes vary between 5 and 20 mA. They reach their peak value within a few nanoseconds and decrease over a few microseconds. Because the Pearson coil response time is about 10 ns, we conclude that the rise time of the current pulse is, at most, 10 ns. The peak electrical power is $P_{\text{in}} \simeq 100$ W. The average power is $\bar{P}_{\text{in}} \leq 1$ W. In a similar setup, but with a $L_S/D = 0.40$ spike, similar electrical features have been recorded and have been attributed to the onset of corona discharge regimes [9]. In particular, in the negative case, current pulses are typical Trichel pulses. Thus, depending on the polarity, the ac circuit generates periodic negative or positive corona discharges. Besides, in both polarities, the mean value of the drag coefficient, C_D, is unchanged when the discharge is on or off. The fluctuating part of the drag signal has not been analyzed because the 50-Hz duty cycle of the ac discharge is difficult to distinguish from the baseline 50-Hz electrical noise recorded on the drag balance signal.

The examination of the flowfield schlieren recordings show that, whenever the negative corona is on, the shock front pulsation is stabilized and reaches a steady configuration. A typical schlieren picture of this configuration is given in Fig. 9. It resembles the schlieren pictures obtained when the flow is stabilized with the rough spike, as in Fig. 7a. When the negative discharge is turned off, the flowfield returns to is baseline unsteady configuration. With the positive discharge, this stabilization is not as clearly seen. To assess the effect of the discharge polarity on the flowfield, we compute the correlation between each image of the fast schlieren recordings and a reference picture of the flowfield. To better spot the stabilization region, we take as reference a picture corresponding to the innermost position of the shock, which is very similar to the stabilized state shown in Fig. 9. Thus, when the shock switches to a steady state, the correlation factor is close to 1 and, when the shock is pulsating, the correlation factor decreases. Figures 10 and 11 show the discharge current, I_D, and voltage, U_D, of both discharges alongside the image

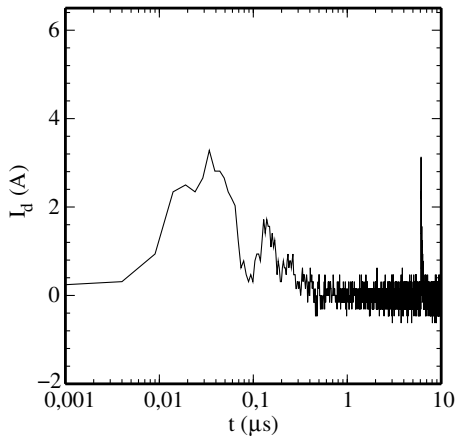

a) Negative discharge, one current pulse, sampling rate 200MHz

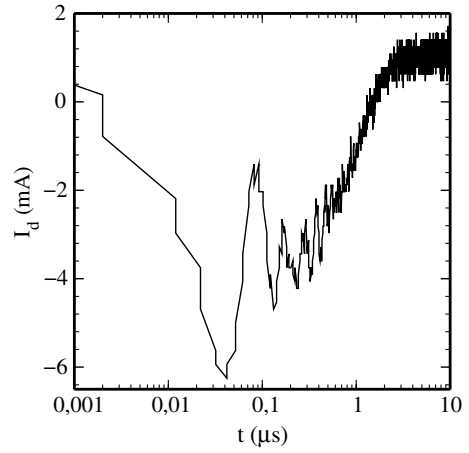

b) Positive discharge, one current pulse, sampling rate 200 MHz

Fig. 8 Typical current pulses in both polarities for $U_D \simeq 7$ kV measured in the $M_0 = 3$ airflow.

correlation for both polarities. In Fig. 10, the spike is negatively biased. When the discharge is on, positive current bursts are recorded. Conversely, in Fig. 11, the spike is positively biased and negative current bursts are recorded when the discharge is on. In both polarities, reverse current pulses are recorded at the discharge cutoff.

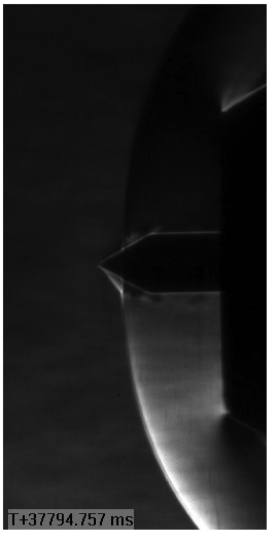

Fig. 9 Typical schlieren picture of a flow stabilized by a pulsed negative discharge ($Re_u \simeq 1.510^7$ m^{-1}, $n_0/n_L = 0.09$, $T_0 = 120$ K).

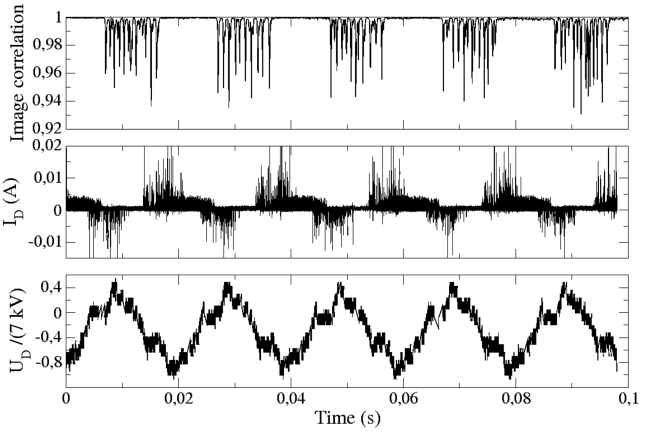

Fig. 10 Image correlation, discharge current, and voltage for the negative discharge ($Re_u = 1.07 \times 10^7$ m^{-1}, $n_0/n_L = 0.09$, $T_0 = 120$ K).

The origin of this phenomenon is unclear. It could be due to the neutralization of the surface charges accumulated when the discharge is on.

Figure 10 shows a clear correlation between the negative discharge onset and the shock wave unsteadiness alleviation. However, the effective alleviation of the shock movements occurs roughly 2 ms after the first current bursts. There is an intermediate regime in which the flow remains unsteady after the discharge is switched on. Note that the voltage signal is noisy because of an unmatched impedance at the probe output. A similar analysis was performed for the positive case. It appears that the discharge does stabilize the shock, but in a much shorter time period, around the peak of discharge voltage. Again, the voltage recording is inaccurate, this time due to a signal saturation. In summary, the negative corona is more efficient than the positive one because the shock unsteadiness alleviation is much longer and better defined.

This difference in efficiency between the negative corona and the positive corona provides a first insight into the mechanism of plasmaflow interaction. Thus, this difference has been investigated by studying the electrical characteristics and emission pattern topologies of both discharges.

First, the measured current traces show that repetitive current pulses occur in both regimes. Although the shape and amplitude of the current pulses are similar in both cases, as shown in Fig. 8, the pulse repetition rate is markedly different depending on the discharge polarity. For a given polarity, the discharge voltage magnitude continuously evolves between 0 and 7 kV. Thus, at a given voltage, it is possible to compute the current pulse periods. Figure 12 displays pulse periods plotted against the spike voltage in both polarities. For the positive corona regime, the pulse periods are scattered around a

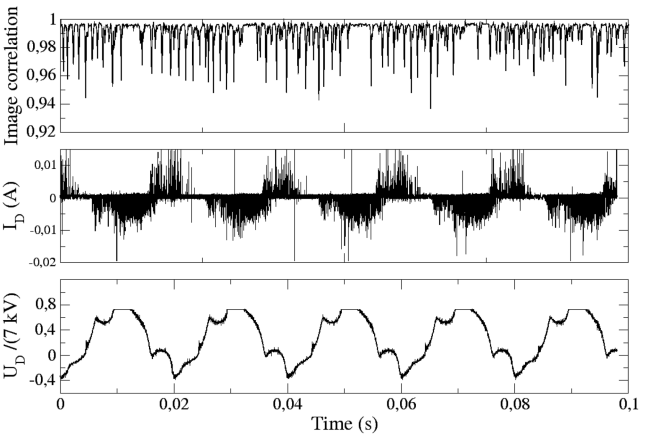

Fig. 11 Image correlation, discharge current, and voltage for the positive corona discharge ($Re_u = 1.06 \times 10^7$ m^{-1}, $n_0/n_L = 0.09$, $T_0 = 120$ K).

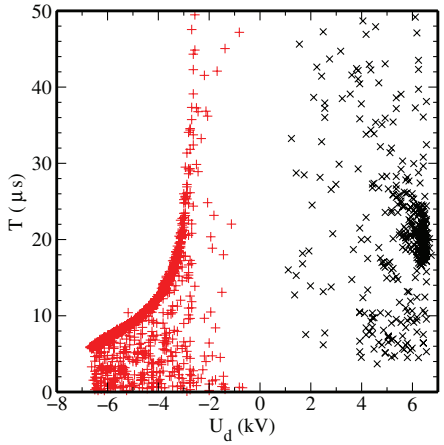

Fig. 12 Current pulse periods, where + represents the negative corona ($n_0/n_L = 0.12$) and × represents the positive corona ($n_0/n_L = 0.12$).

mean value of about 20 μs for $U_D \simeq 4$ kV. No voltage dependency is noticed. For the negative corona, pulse periods are much less scattered. For a given voltage, there is a threshold value that decreases when the voltage magnitude increases. This demonstrates that negative current pulses are more regular than positive current pulses and that their lower frequency is roughly proportional to the voltage magnitude. This behavior, typical of Trichel pulses, has been also observed in a steady flowfield [9].

Second, the emission patterns of the discharge during a single pulse are observed. Emission patterns are recorded using an ICCD imaging camera and a photon multiplier tube (PMT), which collects the light emitted in the vicinity of the spike tip. The PMT signal shows sharp pulses synchronized with the current pulses. This indicates that the current pulses and the light emission are strongly correlated. By setting the ICCD exposure time close to the mean pulse period, around 20 μs, it is possible to record a single or a few pulses. Figure 13a shows typical images obtained with the ICCD camera in both polarities. The test-model outline is superimposed in each case. In the negative case, the ICCD picture in Fig. 13a shows that the emitting region during a single pulse is located near the spike tip and has a diffuse shape. On the contrary, in the positive case, although the current pulses have a similar shape, the ICCD pictures show filamentary patterns attached to the tip. For a single pulse, only one filament can be seen. These filaments are randomly distributed, as shown in 13b in which the exposure time is increased to 100 μs to show several filaments. Light emission is a sign of electronic excitation. Thus, the filaments indicate that, in the positive case, electrons flow in narrow channels. Thus, electrical characteristics and emission patterns underscore the differences between the negative and positive corona regimes. The negative regime is made of regular Trichel pulses and its emission pattern is diffuse. The positive regime is made of less regular pulses, with a filamentary emission pattern, that suggest the presence of positive streamers.

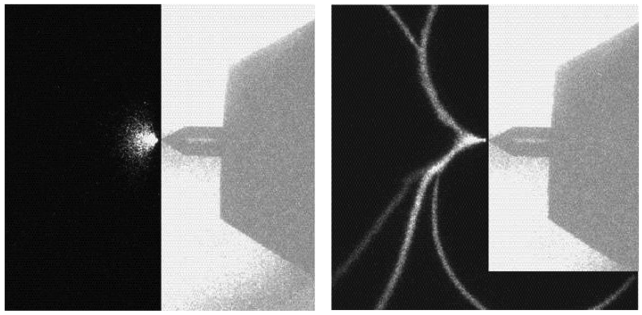

a) Negative discharge, exposure time ≃ 8 μs, one current pulse only

b) Positive discharge, exposure time = 100 μs, several current pulses

Fig. 13 ICCD pictures of the discharge.

Although insufficient to explain the difference in the efficiency of the two regimes, these results must be taken into account in any physical picture proposed to explain the stabilization mechanism.

To propose a hypothesis capable of explaining the stabilization mechanism, it is necessary to understand how the flow can be modified by the discharge. Because most of the experiments mentioned in the Introduction have found an explanation thanks to the heating hypothesis [1,2], the search for the effective mechanism in the pulsation alleviation phenomenon should first focus on the heating of the gas by the plasma. Bletzinger et al. [2] distinguish two types of heating: volume and surface heat deposition. We assess the possible effect of these two deposition modes in our particular case using an order-of-magnitude analysis and an infrared imaging technique. Because of the limitations of these approaches, we can only estimate the effect of a continuous heat deposition.

First, volume gas heating may occur through the fast dissociative quenching of the excited electronic states of N_2 or the slower deexcitation of the vibrational modes of N_2 or O_2 by vibrational–translational energy transfer. In our case, we cannot assess the relative importance of these two processes because the concentrations of the various species intervening in the process were not measured. However, we can model the effect of fast quenching by supposing that all the electric power is transferred instantly to the translational/rotational degrees of freedom. Thus, we can roughly estimate the effect of fast quenching on the flow temperature. To this end, we assume that the heating is continuous. The average heating power is at most 1 W in the negative case. As shown in Fig. 13a, the excitation region occupies a small volume that can be modeled as a 3-mm-diam cylinder of length $L = 3$ mm. An energy balance on this cylinder gives

$$\rho_0 u_0 c_p (T_0 + \Delta T) S = P_{\text{in}} + \rho_0 u_0 c_p T_0 S \tag{2}$$

where $S = \pi R^2$ is the cylinder cross section. Here, we have simplified the problem by considering that the flow density ($\rho_0 \simeq 0.13$ kg · m^{-3}) and velocity ($u_0 \simeq 650$ m · s^{-1}) are constant. Thus, we have

$$\Delta T = \frac{P_{\text{in}}}{\rho_0 u_0 c_p S} \simeq 2 \text{ K}$$

It follows that the net temperature increase through dissociative quenching is low. Thus, the hypothesis of a constant flow density and velocity is correct, because the relative temperature variations are very weak, of the same order of magnitude as the baseline flow temperature. It is highly improbable that such a low temperature increase could stabilize the flow. Besides, this is a limiting case in which all the input power directly heats the gas. In reality, most of the power goes to the slowly decaying vibrational energy modes, thus lowering the computed temperature increase. Consequently, we conclude that continuous volume heating cannot be responsible for the flow stabilization.

Second, heating in a thin region, or surface heating, could be strong because all the power is channeled in a small volume. Recently, Ito and Cappelli [16] estimated a temperature rise of roughly 400 K in the cathode layer of argon microdischarges at a pressure of around 10 Torr and an input power of a few watts. Although these results were obtained with a different type of discharge and for a larger current density, they suggest that strong heating in the cathode layer is possible. In the case of a negative corona discharge, the numerical computations of Morrow [17] indicate that a cathode layer is formed during the pulse and slowly decays in the recovery period. The formation of a cathode layer in the case of a corona discharge and the measurements of Ito and Cappelli suggest that a strong heating at the spike tip is possible. To investigate this point, an infrared camera was used to record the spike surface temperature during a run in which corona discharges were generated with a dc power supply. Three cases are considered. In the reference case, no discharge is generated. In the second case, with the same flow conditions, a negative discharge is generated with the dc power supply turned on 4 s after the flow onset. In the third case, the

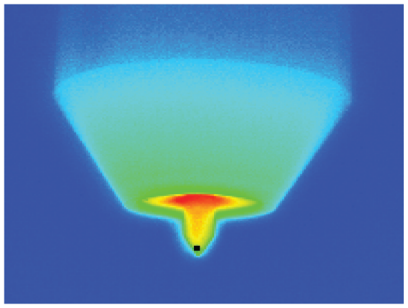

Fig. 14 Typical IR image. The location of the surface temperature measurement on the spike tip is marked by a black dot.

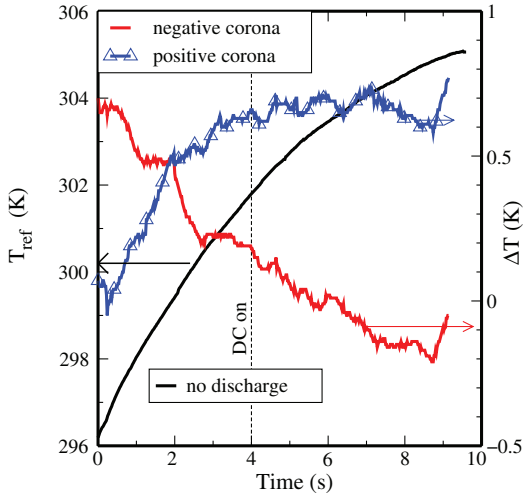

Fig. 15 The black line represents the surface temperature (T_{ref}) evolution in the reference case ($Re_u = 1.22 \times 10^7$ m^{-1}, $n_0/n_L = 0.125$). The red line represents the ⊖ spike deviation from T_{ref} ($Re_u = 1.27 \times 10^7$ m^{-1}, $n_0/n_L = 0.129$). The blue line represents the ⊕ spike deviation from T_{ref} ($Re_u = 1.21 \times 10^7$ m^{-1}, $n_0/n_L = 0.124$).

same procedure is repeated, this time with a positive discharge. In all cases, the surface temperature evolution is monitored at the spike tip, as shown in Fig. 14. Figure 15 presents the surface temperature deviations from the reference surface temperature during the runs in which the positive and negative coronas were generated. There is no clear surface temperature increase when the discharge is turned on. During the entire run, the deviation is, at most, three quarters of a Kelvin in both cases. This value is below the stagnation temperature deviation from run to run, around 1 K. This means that either the surface temperature increase is below the stagnation temperature deviation (around 1 K) or the IR camera time resolution (25 fps) is insufficient to resolve transient temperature increases. In either case, we conclude that continuous surface heating is negligible.

Thus, the lack of evidence of a continuous heating, either in volume or in surface, is not surprising. In fact, the average corona electrical input power is rather low, around 100 mW. Moreover, in corona discharges, most of the input power is channeled and stored in the vibrational energy modes. Hence, on average, only a few milliwatts are actually spent to heat the gas. Nevertheless, this does not discard the heating hypothesis. In fact, the peak electrical input power during the pulse can reach up to 100 W. In this case, even if 99% of the input power goes into slowly decaying energy modes, 1 W is spent to heat the gas. Part of this power, via the joule effect, heats the gas in the thin cathode layer at the spike tip surface. Thus, although the average power effectively spent to heat the gas is low, it is possible that instantaneous heating could be quite high during the current pulses. To illustrate this point, an analysis of the energy balance equation allows us to compute an estimate of the heating rate during the pulse. With the same notation as in Eq. (2), we have

$$\frac{\delta T}{\delta t} \sim \frac{P_{\text{in}}}{\rho_0 c_p S L} \tag{3}$$

We assume that the heating lasts approximately for the duration of the pulse, about $\delta t \simeq 100$ ns, as shown in Fig. 8. If the heating is uniformly deposited in the volume defined for Eq. (2), we can see that even for $P_{\text{in}} \simeq 100$ W, the temperature increase is negligible ($\delta T < 4$ K). However, if we consider the case of a surface heating modeled by a thin cylinder of length $L = 100$ μm, we have $\delta T \sim 10^2$ K. It is possible that, in the case of surface heating, the heat deposition area, S, is even smaller. Consequently, even if 99% of the input power goes into the vibrational energy modes, a significant temperature increase can still be obtained. This pulsed heating might explain the flow stabilization and should be further investigated with fast infrared diagnostics.

V. Possible Mechanism

The effects of small surface defects or a higher Reynolds number on the stabilization of the shock front without plasma have been demonstrated in Sec. III. In these two cases, the schlieren pictures of the stabilized shock, shown in Fig. 7, are very similar to the schlieren picture of the flow with the shock stabilized by the negative corona, shown in Fig. 9. This suggests that the negative corona discharge has the same effect as a higher Reynolds number or the small surface defects. Thus, we propose the following hypothesis: the negative corona discharge triggers the transition to turbulence in the spike boundary layer, owing to small pressure surges caused by regular, pulsed heating in the discharge cathode layer, resulting in pulsed pressure surges. The pulsed discharge would then act as a pulsed acoustic source.

This assumption is borne out by several sources in the literature that suggest that the transition to turbulence could be triggered by a regular acoustic excitation.

Mack [18] showed that there are two linearly unstable modes in a supersonic boundary layer. The exponential growth of these modes can lead to the transition to turbulence. Reshotko summarizes the different stages of the transition to turbulence in a sketch presented in [19], Fig. 1. The first stage involves the channeling of external perturbation energy into the boundary-layer unstable modes. The channeling mechanism, termed receptivity, has been studied by Ma and Zhong in the case of a $M_0 = 4.5$ flat plate [20] or a $M_0 = 7.99$ cone. They showed that the energy of external acoustic perturbation is transmitted to the unstable mode via resonant interaction. But, more important, the order of magnitude of the frequency of this perturbation or of the unstable Mack modes are of a few tens of kilohertz, which is close to the typical Trichel pulse frequency, around 50–100 kHz. According to Reshotko [19], depending on the external perturbation energy, exponential or transient growth can occur. If the energy is high enough, the perturbation can trigger a bypass mechanism, leading to an anticipated transition to turbulence for Reynolds numbers much lower than a natural transition. In a wind tunnel, bypass transition is a problem because transition on the test model occurs earlier than in real flight conditions. This is due to the strong perturbation levels radiated by the nozzle turbulent boundary layer [13]. These effects have spurred the search for a so-called quiet wind tunnel. Thus, in our case, the pulsed heating at the spike tip possibly generates a strong acoustic perturbation that couples with the unstable Mack modes via resonant interaction, thereby triggering the transition to turbulence. It is worth noting that Maslov et al. [21] have already employed plasma discharges as acoustic sources to probe the receptivity of a supersonic boundary layer. Following this hypothesis, several observations can be explained. First, positive discharges are less efficient than negative discharges because they are less regular and, thus, couple less efficiently with the boundary-layer modes. Thus, even if the peak power in the positive case is larger, the irregular occurrence of the pulse prevents an efficient coupling with the boundary-layer modes. Second, the unsteadiness of the flow for a short period of time after the discharge is turned on could be due to the fact the discharge repetition rate is not high enough nor regular enough to efficiently disturb the boundary layer.

To further test these assumptions and assess the validity of this hypothesis, onboard unsteady pressure measurements should be conducted.

In fact, the mechanism of the shock wave stabilization with Trichel discharges is open to speculation. Other appealing hypotheses can be proposed, such as the effect of tangential jets generated by the discharge or an anomalous turbulence intensity increase in the ionized gas. The hypothesis we propose here has the advantage of explaining on simple terms several observations made in the course of these experiments

VI. Conclusions

The goal of the present work was to study plasmaflow interactions at $M_0 = 3$ with time-resolved diagnostics using a model and a power supply design proposed by Kuo et al. [7] and Kuo and Bivolaru [8]. The flow around the model is unsteady for a reduced spike length $L_S/D = 0.46$ below a critical Reynolds number. It becomes steady above a critical Reynolds number or if small surface defects are machined on the spike tip. This suggests that the transition to turbulence is able to stabilize the shock front, possibly because the state of the boundary layer affects the detachment point location. While generating a discharge in the flow, neither a dispersion of the shock wave nor a decrease of the mean drag coefficient have been recorded. In this sense, this experiment does not reproduce Kuo and Bivolaru's observations. Nevertheless, when a corona discharge is generated in the unsteady case, we observe that the shock front is stabilized, with a stronger effect in the negative case than in the positive case. The negative corona discharge is made of regular Trichel pulses, whereas the positive corona is made of less regular filamentary patterns, likely positive streamers. The mechanism of the plasma-induced stabilization was investigated, mainly by considering the heating hypothesis. If we assume that the discharge continuously heats the gas, an order-of-magnitude analysis shows that volume heating is negligible (<2 K). Infrared images show no significant increase in the surface temperature of the spike tip, indicating that continuous surface heating is also negligible. Hence, it is probable that pulsed heating might be at work in the discharge. To explain the stabilization of the flow by the discharge, we propose a possible mechanism by which the discharge acts as a pulsed acoustic source, owing to transient heating in the cathode layer. This acoustic perturbation is strong enough to trigger a bypass transition mechanism, leading to an anticipated transition to turbulence. Thus, the flow becomes steady, as if the Reynolds number were higher or small surface defects were present at the spike tip. This is supported by the fact that the discharge has the same effect as the small surface defects that trigger the transition to turbulence. This mechanism is able to explain the experimental observations made in the course of this study.

To prove this hypothesis, it would be necessary to probe the state of the spike boundary layer using time-resolved pressure measurements. If confirmed, it would mean that the discharge behaves as an actuator capable of triggering the transition to turbulence with a fast response time. Such a device could be useful for controlling the state of an otherwise laminar boundary layer, for which turbulence might be required in a certain situation, for example, to prevent flow detachment.

Acknowledgments

This work is part of the ONERA PUMA Research Program. The authors would like to thank the team at the R1Ch wind tunnel for its expert assistance.

References

[1] Fomin, V., Tretyakov, P., and Taran, J.-P., "Flow Control Using Various Plasma and Aerodynamic Approaches (Short Review)," *Aerospace Science and Technology*, Vol. 8, No. 5, 2004, pp. 411–421. doi:10.1016/j.ast.2004.01.005

[2] Bletzinger, P., Ganguly, B., VanWie, D., and Garscadden, A., "Plasmas in High Speed Aerodynamics," *Journal of Physics D: Applied Physics*, Vol. 38, No. 4, 2005, pp. R33–R57. doi:10.1088/0022-3727/38/4/R01

[3] Palm, P., Meyer, R., and Plönjes, E., "Nonequilibrium Radio Frequency Discharge Plasma Effect on Conical Shock Wave: $M = 2.5$ Flow," *AIAA Journal*, Vol. 41, No. 3, 2003, pp. 465–469.

[4] Shang, J., "Plasma Injection for Hypersonic Blunt-Body Drag Reduction," *AIAA Journal*, Vol. 40, No. 6, June 2002, pp. 1178–1186.

[5] Bivolaru, D., and Kuo, S., "Aerodynamic Modification of Supersonic Flow Around Truncated Cone Using Pulsed Electrical Discharges," *AIAA Journal*, Vol. 43, No. 7, July 2005, pp. 1482–1489. doi:10.2514/1.7361

[6] Bivolaru, D., and Kuo, S., "Observation of Supersonic Shock Wave Mitigation by Plasma Aero-Spike," *Physics of Plasmas*, Vol. 9, No. 2, Feb. 2002, pp. 721–723. doi:10.1063/1.1433662

[7] Kuo, S., Kalkhoran, I., Bivolaru, D., and Orlick, L., "Observation of Shock Wave Elimination by a Plasma in a Mach = 2.5 Flow," *Physics of Plasmas*, Vol. 7, No. 5, 2000, pp. 1345–1348. doi:10.1063/1.873776

[8] Kuo, S., and Bivolaru, D., "Plasma Effect on Shock Waves in a Supersonic Flow," *Physics of Plasmas*, Vol. 8, No. 7, 2001, pp. 3258–3263. doi:10.1063/1.1376422

[9] Elias, P. Q., Chanetz, B., Larigaldie, S., and Packan, D., "Experimental and Theoretical Study of the Effect of Glow Discharge Generated Near a $M = 3$ Steady Bow Shock,"*AIAA Journal*, Vol. 19, No. 6, 2007, pp. 1007–1017.

[10] Elias, P. Q., Chanetz, B., Coponet, D., Benay, R., Packan, D., and Larigaldie, S., "On Board Plasma Generation on a Supersonic Pulsating Airflow," *40eme Colloque d'Aérodynamique Appliquée*, Association Aeronautique et Astronautique de France, Paris, March 2005.

[11] Mair, W., "Experiments on Separation of Boundary Layers on Probes in Front of Blunt-Nosed Bodies in a Supersonic Air Stream," *Philosophical Magazine*, Vol. 43, No. 342, 1952, pp. 695–716.

[12] Feszty, D., Badcock, K. J., and Richards, B. E., "Driving Mechanisms of High-Speed Unsteady Spiked Body Flows, Part 1: Pulsation Mode," *AIAA Journal*, Vol. 42, No. 1, 2004, pp. 95–106. doi:10.2514/1.9034

[13] Benay, R., and Chanetz, B., "Design of Boundary Layer Suction Device for a Supersonic Quiet Wind Tunnel by Numerical Simulation," *Aerospace Science and Technology*, Vol. 8, No. 4, June 2004, pp. 255–271. doi:10.1016/j.ast.2003.11.003

[14] Van Driest, E., and Blumer, C., "Boundary Layer Transition at Supersonic Speeds: Three-Dimensional Roughness Effects (Spheres)," *Journal of Aerospace Science*, Vol. 29, No. 8, 1962.

[15] Chapman, D. R., Kuehn, D. M., and Larson, H. K., "Investigation of Separated Flows in Supersonic and Subsonic Streams with Emphasis on the Effect of Transition," NACA TN 3869, 1957.

[16] Ito, T., and Cappelli, M. A., "Ion Energy Distribution and Gas Heating in the Cathode Fall of a Direct-Current Microdischarge," *Physical Review E (Statistical Physics, Plasmas, Fluids, and Related Interdisciplinary Topics)*, Vol. 73, April 2006, pp. 46401–1–9. doi: 10.1103/PhysRevE.73.046401

[17] Morrow, R., "Theory of Negative Corona in Oxygen," *Physical Review A*, Vol. 32, No. 3, 1985, pp. 1799–1809. doi:10.1103/PhysRevA.32.1799

[18] Mack, L., "On the Application of Linear Stability Theory to the Problem of Supersonic Boundary-Layer Transition," AIAA Paper 74-134, 1974.

[19] Reshotko, E., "Transient Growth: A Factor in Bypass Transition," *Physics of Fluids*, Vol. 13, May 2001, pp. 1067–1075. doi:10.1063/1.1358308

[20] Ma, Y., and Zhong, X., "Receptivity of a Supersonic Boundary Layer Over a Flat Plate. Part 1. Wave Structure and Interaction," *Journal of Fluid Mechanics*, Vol. 488, July 2003, pp. 31–78. doi:10.1017/S0022112003004786

[21] Maslov, A. A., Shiplyuk, A. N., Sidorenko, A. A., and Arnal, D., "Leading-Edge Receptivity of a Hypersonic Boundary Layer on a Flat Plate," *Journal of Fluid Mechanics*, Vol. 426, Jan. 2001, pp. 73–94. doi:10.1017/S0022112000002147

N. Chokani
Associate Editor